Bardoxolone methyl inhibits ferroptosis through the Keap1-Nrf2 pathway in renal tubular epithelial cells

SOYEON YOO[1,2], MIYEON KIM[1,2], JU YOUNG BAE[1], SANG AH LEE[1,2] and GWANPYO KOH[1,2]

[1]Department of Internal Medicine, Jeju National University College of Medicine, Jeju 63241, Republic of Korea; [2]Department of Internal Medicine, Jeju National University Hospital, Jeju 63241, Republic of Korea

Received April 23, 2025; Accepted July 3, 2025

DOI: 10.3892/mmr.2025.13632

Abstract. Diabetic kidney disease (DKD), a primary cause of end-stage kidney disease, involves ferroptosis in renal tubular epithelial cells (RTECs). Bardoxolone methyl (BM), known for its antioxidant and anti-inflammatory properties, activates the Keap1-Nrf2 pathway and has slows kidney function decline. 2-Deoxy-D-ribose (dRib) can induce ferroptosis in RTECs by promoting the degradation of solute carrier family 7 member 11 (SLC7A11), a protein essential for cystine transport and glutathione (GSH) synthesis. The present study aimed to evaluate whether BM could inhibit dRib-induced ferroptosis in RTECs and to elucidate the underlying mechanisms. Using NRK-52E cells and primary RTECs, cystine uptake, GSH and iron levels, cell viability, lipid peroxidation and ferroptosis-related markers were assessed. Co-immunoprecipitation was used to assess Keap1-Nrf2 interactions and confocal microscopy was employed to observe Nrf2 nuclear translocation. BM pretreatment dose-dependently restored cystine uptake, increased GSH levels and improved cell viability, while reducing intracellular iron accumulation and lipid peroxidation triggered by dRib. These protective effects were attenuated by Nrf2 inhibitors, indicating that the activity of BM is Nrf2-dependent. BM enhanced Nrf2 protein expression, upregulated SLC7A11 and increased the expression of Nrf2-ARE target genes, including heme oxygenase-1, NADPH quinone oxidoreductase 1, glutamate-cysteine ligase catalytic subunit and glutamate-cysteine ligase modifier subunit, while suppressing ferroptosis-related markers (acyl-CoA synthetase long chain family member 4, ChaC glutathione-specific gamma-glutamylcyclotransferase 1 and prostaglandin-endoperoxide synthase 2). Furthermore, BM disrupted the Nrf2-Keap1 interaction, promoting Nrf2 nuclear translocation. In conclusion, BM may disrupt the Keap1-Nrf2 interaction in RTECs, upregulate SLC7A11 and mitigate dRib-induced ferroptosis, thereby presenting a potential therapeutic option to prevent the progression of DKD by protecting RTECs from ferroptosis.

Correspondence to: Professor Gwanpyo Koh, Department of Internal Medicine, Jeju National University College of Medicine, 15 Aran 13-gil, Jeju 63241, Republic of Korea
E-mail: okdom@jejunu.ac.kr

Key words: bardoxolone methyl, ferroptosis, Keap1-Nrf2 pathway, diabetic kidney disease, SLC7A11

Introduction

Ferroptosis is a regulated form of cell death distinct from necrosis, apoptosis, pyroptosis, and autophagy. It is characterized by iron-dependent oxidative damage and lipid peroxidation (1,2). The term 'ferroptosis' was first introduced by Dixon *et al* (3) in 2012. This form of cell death can be inhibited by iron chelators such as deferoxamine (DFO) and radical-trapping antioxidants like ferrostatin-1 (Fer-1) and liproxstatin-1 (Lip-1) (4,5). A key step in the prevention of ferroptosis is the synthesis of glutathione (GSH), which requires intracellular cystine uptake via the system χc- on the cell membrane (6). Consequently, inhibitors of system χc- such as erastin are well-established inducers of ferroptosis (3).

Recently, we reported that 2-deoxy-D-ribose (dRib) also induces ferroptosis in renal tubular epithelial cells (RTECs) by increasing the ubiquitination and proteasomal degradation of solute carrier family 7 member 11 (SLC7A11), a functional subunit of system χc- (7). Ferroptosis has been implicated in the pathogenesis of various diseases, including cancer, ischemia/reperfusion injury, chronic neurodegenerative diseases, and acute kidney injury (8,9).

Diabetic kidney disease (DKD), which affects 20-40% of patients with diabetes, is the most common cause of end-stage kidney disease (10). Although angiotensin-converting enzyme inhibitors, angiotensin receptor blockers, sodium-glucose co-transporter 2 inhibitors, and nonsteroidal mineralocorticoid receptor antagonists have been shown to slow the progression of DKD, patients often still develop chronic kidney disease (CKD) and require dialysis (11,12). This highlights the urgent need for more effective therapies to treat DKD. Ferroptosis, a regulated form of cell death, has recently been identified as a key factor in the progression of DKD, particularly in renal tubular epithelial cells (RTECs) (13,14). In patients with DKD, serum ferritin levels are elevated, whereas the mRNA expression of SLC7A11 and GPX4 in kidney tissue is decreased-a molecular pattern strongly associated with ferroptosis (15,16). Similarly, in animal models of DKD, kidney tissues showed increased levels of malondialdehyde (MDA), a marker of lipid peroxidation, and elevated expression of acyl-CoA

synthetase long-chain family member 4 (ACSL4), a known ferroptosis marker (17). Moreover, studies by Wang *et al* (18) and Li *et al* (19) have demonstrated clear signs of ferroptosis, such as iron overload and increased reactive oxygen species (ROS) from lipid peroxidation, in kidney tissues from streptozotocin-induced diabetic mice and in RTECs exposed to high glucose levels.

Bardoxolone methyl (BM) is a synthetic triterpenoid derived from the natural compound oleanolic acid and possesses antioxidant and anti-inflammatory properties. The primary mechanism of BM involves disrupting the interaction between nuclear factor erythroid 2-related factor 2 (Nrf2) and Kelch-like ECH-associated protein 1 (Keap1), thereby activating the intracellular Nrf2 signaling pathway. This prevents Nrf2 degradation, promotes its nuclear translocation, and enables it to bind to antioxidant response elements (ARE) in the promoter regions of target genes, thereby regulating their expression (20,21). Genes regulated by the Nrf2-ARE pathway include heme oxygenase-1 (HO-1), NADPH quinone oxidoreductase 1 (NQO1), and γ-glutamate cysteine ligase (GCL) (22). In addition, SLC7A11, a crucial component in ferroptosis inhibition, is also regulated by Nrf2 (23).

Clinical studies involving patients with type 2 diabetes and CKD have shown the renoprotective effects of BM. In an open-label, single-arm study, BM significantly increased estimated glomerular filtration rate (eGFR) from baseline (24), and randomized controlled trials also showed improvements in eGFR compared to baseline and placebo groups (25-27). These findings highlight the potential of BM as a novel therapeutic option for DKD (28).

The aim of our study was to investigate the protective mechanisms of BM on RTECs in the context of DKD. Specifically, we attempted to determine how BM inhibits ferroptosis in RTECs, which contributes to DKD progression. We explored the ability of BM to preserve RTEC viability and its mechanisms of action when ferroptosis is induced by dRib-mediated system χc- disruption. By elucidating the molecular mechanisms through which BM suppresses ferroptosis in RTECs, our findings provide valuable insights into the development of novel therapeutic strategies for DKD.

Materials and methods

Cell culture. The NRK-52E cell line, a proximal tubular epithelial cell line derived from rats, was provided by Prof. Sang-Ho Lee from Kyung Hee University College of Medicine. The cells were cultured in Dulbecco's Modified Eagle Medium (DMEM) supplemented with 10% fetal bovine serum (FBS), 100 mg/ml penicillin, and 100 mg/ml streptomycin under a 5% CO_2 and 95% O_2 environment. The culture medium was replaced with fresh medium every 2 days. When the cells reached 70% confluence, they were subcultured after treatment with trypsin.

To confirm the reproducibility of the experimental results obtained from NRK-52E cells, primary cultures of rat proximal tubular epithelial cells were also established and used for experiments. Sprague Dawley rats (approximately 10 weeks old) were euthanized using carbon dioxide (CO_2) inhalation in accordance with the protocol approved by the Institutional Animal Care and Use Committee of Jeju National University (protocol no. 2024-0088; approval no. 2022-0014). The animals were placed in a dedicated sealed chamber, and CO_2 was introduced at a displacement rate of 30% of the chamber volume per minute until the concentration reached 60-70%. After the concentration was raised, the chamber was gently shaken up and down to maintain an appropriate CO_2 level. Following euthanasia, death was confirmed by checking for the cessation of heartbeat, after which the kidneys were removed. The kidneys were washed with Hanks' Balanced Salt Solution (HBSS), the renal capsule was removed, and the kidneys were dissected into four pieces, isolating only the cortical tissue. The HBSS was then removed, and the tissue was washed with cold phosphate-buffered saline (PBS). The washed tissue was transferred to a trypsin-treated flask, and 20 ml of a solution containing DNase I (1 mg/ml) and Collagenase Type I (2 mg/ml) in HBSS was added. The tissue was then sequentially passed through sieves of different pore sizes to remove distal tubule and glomerular cells. The proximal tubule cell suspension in HBSS was centrifuged at 228 x g (1,000 rpm) for 10 min, and the collected cells were cultured in rat tail collagen-coated plastic ware. After 1 week, the cells were harvested for intracellular L-[^{14}C]cystine uptake assays, intracellular GSH content measurement, and lactate dehydrogenase assays.

Measurement of intracellular cystine transport. NRK-52E cells ($3x10^5$ cells/well) or an equivalent number of isolated RTECs were seeded into 24-well cell culture plates and cultured in DMEM medium containing 10% FBS for 2 days. After removing the culture medium, the cells were washed with 500 µl of extracellular fluid (ECF) buffer, pre-warmed to 37˚C, and composed of 122 mM NaCl, 25 mM $NaHCO_3$, 3 mM KCl, 1.4 mM $CaCl_2$, 1.2 mM $MgSO_4$, 0.4 mM K_2HPO_4, 10 mM D-glucose, and 10 mM HEPES (pH 7.4). The cells were then stimulated for 4 h with dRib, BM, ML385, or brusatol. During the final 1 h of stimulation, 500 µl of 37˚C ECF buffer containing 0.1 µCi L-[^{14}C] cystine (1.7 µM) was added to each well to induce intracellular uptake of L-[^{14}C]cystine. After incubation, the buffer was completely removed, and the cells were washed with cold, radioisotope-free ECF buffer to terminate the uptake process. The cells were lysed with 750 µl of 1% Triton X-100 in Dulbecco's phosphate-buffered saline, after which 500 µl of the lysate was mixed with 5 ml of scintillation cocktail for radioactivity measurement using the Wallac MicroBeta TriLux 1450 Liquid Scintillation and Luminescence Counter (PerkinElmer, San Juan, PR, USA). The remaining cell lysate was used to determine protein concentration using bicinchoninic acid protein assay kit (Pierce, Rockford, IL, USA). Intracellular L-[^{14}C]cystine uptake was expressed as counts per minute (cpm) per microgram of protein, normalized to total protein concentration.

Measurement of intracellular GSH levels. Intracellular GSH levels were measured using a GSH Assay Kit (Cayman, Ann Arbor, MI, USA) based on the enzymatic recycling method using glutathione reductase. Briefly, NRK-52E cells ($3x10^5$ cells/well) or an equivalent number of isolated RTECs were seeded into 24-well cell culture plates and cultured in DMEM medium containing 10% FBS for 2 days. The cells

were then stimulated for 6 h with dRib, BM, ML385, or brusatol. Following treatment, the cells were lysed by sonication, and the lysates were centrifuged to obtain the supernatant. The GSH concentration in the supernatant was measured according to the manufacturer's instructions. Intracellular GSH levels were normalized to total protein concentration and expressed as nmol/mg protein.

Measurement of intracellular iron levels. Intracellular iron levels were measured using the Iron Assay Kit (Sigma-Aldrich, St. Louis, MO, USA), a colorimetric assay. NRK-52E cells were seeded at a density of $1x10^6$ cells/well in a six-well culture plate and maintained in DMEM supplemented with 10% FBS. The cells were treated simultaneously with dRib, BM, ML385, or brusatol and incubated for 6 h. Subsequently, the cells were lysed using sonication, and the supernatant was collected after centrifugation. Total iron levels were measured according to the manufacturer's protocol. Intracellular iron levels were normalized to the total protein concentration of the cells and expressed as nmol/mg·protein.

Assessment of cell viability. Cytotoxicity was first assessed using a lactate dehydrogenase assay. NRK-52E cells were seeded at a density of $1x10^5$ cells/well in a 96-well cell culture plate, whereas isolated RTECs were plated at an equal number of cells per well in the same type of plate. The cells were maintained in DMEM supplemented with 10% FBS and treated simultaneously with dRib, BM, ML385, or brusatol for 6 h. Cytotoxicity was then measured using the Cytotoxicity Detection KitPLUS (Roche, Mannheim, Germany), and calculated using the following formula: (((experimental value - background control)-(low control - background control))/((high control - background control)-(low control - background control))) x 100. Finally, cell viability (% control) was expressed as: Cell viability (% control)}=100 - cytotoxicity (%).

Measurement of intracellular MDA levels. We selected MDA as a marker to evaluate intracellular lipid peroxidation. NRK-52E cells were seeded in a six-well culture plate at a density of $1x10^6$ cells/well and cultured in DMEM medium containing 10% FBS for 48 h. The cells were then stimulated with dRib, BM, ML385, or brusatol simultaneously for 6 h. Subsequently, MDA levels were measured from the cell lysate using the EZ-Lipid Peroxidation Assay Kit (DoGenBio, Seoul, South Korea). The intracellular MDA levels were normalized to the total protein concentration of the cells and expressed as nmol/mg·protein.

Assessment of lipid ROS levels. Intracellular lipid peroxide levels were measured using flow cytometry with C11-BODIPY dye (Molecular Probes, Eugene, OR, USA). NRK-52E cells were seeded in a six-well culture plate at a density of $1x10^6$ cells/well and cultured in DMEM medium containing 10% FBS. The cells were then stimulated simultaneously with dRib, BM, ML385, or brusatol and incubated for 6 h. During the last 30 min, the cells were treated with 4 μM C11-BODIPY, followed by harvesting using 0.05% trypsin. The collected cells were centrifuged, resuspended in PBS, and analyzed for intracellular lipid ROS levels using a FACScan instrument (BD Bioscience, San Jose, CA, USA). A total of 10,000 cells per sample were analyzed, and the results were expressed as the ratio (fold) of the mean fluorescence intensity relative to the unstimulated control group.

RNA isolation and reverse transcription-quantitative polymerase chain reaction (RT-qPCR). All RT-qPCR experiments were performed in accordance with the Minimum Information for Publication of Quantitative Real-Time PCR Experiments (MIQE) guidelines (29). Total RNA was extracted from cells using TRIzol® (Gibco Invitrogen, Grand Island, NY, USA) according to the manufacturer's instructions. Reverse transcription was performed using 2 μg of RNA with MMLV reverse transcriptase (MGmed Corporation, Seoul, Korea), oligo (dT)15 primer, dNTP (10 mM), and 40 units/μl RNase inhibitor (MGmed Corporation). RT-qPCR was conducted using the KAPA SYBR® FAST qPCR Master Mix (KAPA Biosystems, MA, USA) and an iQTM 5 Multicolor Real-Time PCR Detection System (Bio-Rad, Hercules, CA, USA). Synthesized cDNA was amplified for 40 cycles at 95˚C for 3 sec, 60˚C for 30 sec, and 72˚C for 30 sec, with an initial cycle at 95˚C for 1 min, using specific primers. All primers were custom-synthesized by Bioneer Corporation (Daejeon, Korea), and their sequences are listed in Table I. Amplification specificity was confirmed by melt curve analysis, which showed a single distinct peak for each primer set. Standard curves generated from 5-fold serial dilutions of cDNA templates were used to determine amplification efficiency. All primer pairs showed amplification efficiencies ranging 92-105%, with R^2 values of >0.99. β-actin was used as a reference gene, and its stability was validated across experimental conditions using NormFinder analysis. All qPCR reactions were performed in triplicate, and results represent the mean of three independent biological replicates.

Western blotting (immunoblotting). Cells were lysed using a lysis buffer, and equal amounts of protein from each group were separated using 10% sodium dodecyl sulfate-polyacrylamide gel electrophoresis and transferred onto a nitrocellulose membrane. The membrane was incubated in Tris-buffered saline containing 0.1% Tween and 3% bovine serum albumin to block non-specific antibody binding. It was then incubated with primary antibodies specific to Nrf2 (#ab92946, Abcam), SLC7A11 (#175186, Abcam), ACSL4 (#MA5-42523, Invitrogen), CHAC1 (#217808, Abcam), and PTGS2 (#12282, Cell Signaling) at 4˚C for 2 h. β-Actin (#A2228, Sigma) was used as a loading control. Afterward, the membrane was incubated with horseradish peroxidase-conjugated secondary anti-rabbit antibody (#PI-1000-1, Vector Laboratories) or anti-mouse antibody (#PI-2000-1, Vector Laboratories) for 2 h. Bands were visualized using Western Lightning™ Plus-Enhanced Chemiluminescence (PerkinElmer).

Co-immunoprecipitation (co-IP) assay. IP was performed using Dynabeads Protein G (#10003D, Thermo Fisher Scientific Inc., Waltham, MA, USA). NRK-52E cells were stimulated and cultured under the specified conditions, then lysed using ultrasonication. After centrifugation,

Table I. Primer sequences used for reverse transcription-quantitative polymerase chain reaction.

Gene	Forward primer, 5'-3'	Reverse primer, 5'-3'
SLC7A11	GACAGTGTGTGCATCCCCTT	GCATGCATTTCTTGCACAGTTC
ACSL4	ATATTCGTCACCACTCACA	AACCTTGCTCATAACATTCTT
CHAC1	GCCCTGTGGATTTTCGGGTA	ATCTTGTCGCTGCCCCTATG
PTGS2	GGGAGTCTGGAACATTGTGAA	GTGCACATTGTAAGTAGGTGGACT
HO-1	ACCCCACCAAGTTCAAACAG	GAGCAGGAAGGCGGTCTTAG
NQO1	AGAAGCGTCTGGAGACTGTCTGG	GATCTGGTTGTCGGCTGGAATGG
GCLC	GCACATCTACCACGCAGTCAAGG	TCAAGAACATCGCCGCCATTCAG
GCLM	CTGGACTCTGTCATCATGGCTTCC	TCCGAGGTGCCTATAGCAACAATC
β-actin	TCCTGGCCTCACTGTCCAC	GGGCCGGACTCATCGTACT

SLC7A11, solute carrier family 7 member 11; ACSL4, acyl-CoA synthetase long chain family member 4; CHAC1, ChaC glutathione-specific gamma-glutamylcyclotransferase 1; PTGS2, prostaglandin-endoperoxide synthase 2; HO-1, heme oxygenase-1; NQO1, NAD(P)H quinone dehydrogenase 1; GCLC, glutamate-cysteine ligase catalytic subunit; GCLM, glutamate-cysteine ligase modifier subunit.

the supernatant containing the cell lysate was collected. Dynabeads were conjugated with anti-Nrf2 antibody (#ab92946, Abcam) and anti-rabbit IgG antibody (#2729s, Cell Signaling) to prepare a bead-antibody mixture. This mixture was incubated with the cell lysate overnight at 4˚C under rotation. The bead-antibody-antigen complex was washed four times with Tris-buffered saline with Tween 20. Lithium dodecyl sulfate sample buffer was then added to the beads, followed by incubation at 92˚C for 5 min to elute the immunoprecipitant. The eluted immunoprecipitant was analyzed and quantified using western blot using anti-Keap1 and anti-Nrf2 antibodies.

Immunofluorescence (IF) staining. NRK-52E cells were cultured on coverslips and divided into three groups: an untreated control group, a group treated with 50 mM dRib for 6 h, and a group treated with 0.2 μM BM and 50 mM dRib for 6 h. The cells were fixed with 4% paraformaldehyde at room temperature for 20 min and then permeabilized using a 0.1% Triton X-100 solution. Subsequently, blocking was performed with 5% bovine serum albumin at room temperature for 45 min. The cells were then incubated overnight at 4˚C with primary antibodies: anti-Nrf2 antibody (1:100, #ab92946, Abcam) and anti-Keap1 antibody (1:100, #D6B12, Cell Signaling). After washing, the cells were incubated at room temperature for 1 h with the secondary antibody, donkey anti-rabbit AlexaFluor 488 (1:300, #ab150073, Abcam). Nuclear counterstaining was performed using 4',6-diamidino-2-phenylindole at a 1:5,000 dilution. The stained cells were visualized using a STELLARIS 5 confocal microscope (Leica, Deerfield, IL, USA). To determine the ratio of Nrf2 fluorescence expressed in the nucleus and cytoplasm, images were analyzed using ImageJ software and displayed the values as a bar graph.

Statistical analysis. All data are presented as mean ± standard deviation. Statistical analyses were performed using SPSS software (version 14.0; SPSS Inc.), and $P<0.05$ was considered to indicate a statistically significant difference. Homogeneity of variance was assessed using Levene's test. When the assumption of equal variances was met ($P>0.05$), one-way ANOVA followed by Tukey's post hoc test was used. When the assumption was violated ($P<0.05$), Welch's ANOVA followed by Dunnett's T3 post hoc test was applied. For comparisons between two groups, an unpaired Student's t-test was used.

Results

BM enhances cystine uptake, GSH content, and cell viability, while reducing intracellular iron and lipid peroxidation in dRib-treated RTECs. When NRK-52E cells were stimulated with dRib, there was a significant, dose-dependent decrease in intracellular cystine uptake, GSH content, and cell viability. However, co-treatment with BM significantly prevented these reductions (Fig. 1). Similarly, in primary cultured rat RTECs, dRib led to decreased cystine uptake, GSH levels and cell viability. These impairments were effectively restored by BM treatment (Fig. S1), indicating its protective effect against dRib-induced cellular damage. This shows that BM prevents cell death by increasing the intracellular transport of cystine in RTECs, thereby restoring GSH levels. Furthermore, intracellular iron levels, a key mediator of ferroptosis, were increased by dRib but were reduced to control levels by BM (Fig. 2C). Similarly, intracellular MDA levels and C11-BODIPY fluorescence, indicators of lipid peroxidation, were elevated by dRib but were nearly restored to control levels by BM (Figs. 2D, 2E and S2). Therefore, BM prevents dRib-induced ferroptosis in RTECs by counteracting the reduction in cystine uptake.

Nrf2 inhibitors abolish the BM-mediated recovery of cystine uptake, GSH content, and cell viability, while reversing the BM-induced reduction in iron levels and lipid peroxidation in dRib-treated RTECs. To determine whether the ferroptosis-inhibitory effect of BM depends on Nrf2 activation, we used the specific Nrf2 inhibitors, ML385 and brusatol. In isolated rat RTECs, ML385 and brusatol significantly attenuated the effects of BM in restoring cystine uptake, GSH content, and viability, which were reduced by dRib (Fig. S1).

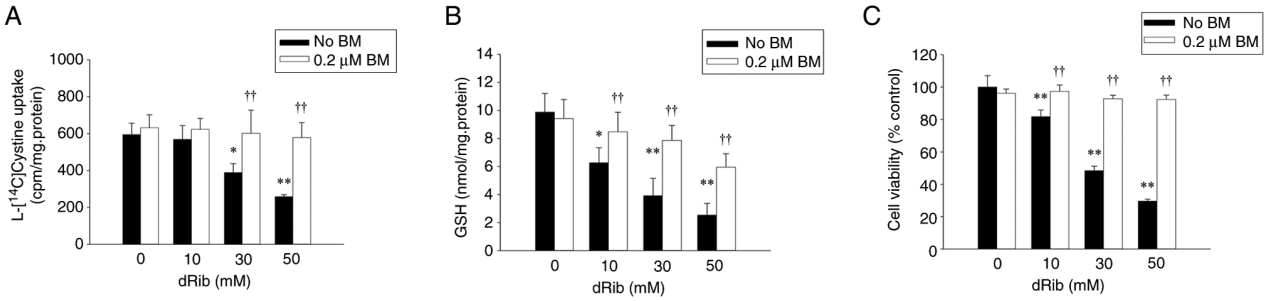

Figure 1. Effects of BM treatment on the dRib-induced decreases in (A) L-[^{14}C]cystine uptake, (B) intracellular GSH content and (C) cell viability. (A) NRK-52E cells were co-stimulated with 0, 10, 30 and 50 mM dRib with or without 0.2 μM BM for 4 h in the extracellular fluid buffer containing 1.7 μM L-[^{14}C]cystine (0.1 μCi/ml) at 37˚C. The radioactivity incorporated into the cells was determined by a liquid scintillation counter. (B and C) The cells were co-stimulated with 0, 10, 30 and 50 mM dRib with or without 0.2 μM BM for 6 h in DMEM containing 10% FBS. (B) Intracellular GSH concentration was measured using a GSH assay kit. (C) Cell viability was measured by LDH release assay. The data are presented as the mean ± SD. These experiments were performed thrice, in triplicate. *P<0.05 and **P<0.01 vs. control and ††P<0.01 vs. dRib alone, as determined by one-way analysis of variance and Tukey's post-hoc test or Welch's ANOVA followed by Dunnett's T3 post hoc test, depending on the result of Levene's test. BM, bardoxolone methyl; dRib, 2-deoxy-D-ribose; GSH, glutathione; LDH, lactate dehydrogenase; DMEM, Dulbecco's Modified Eagle Medium; FBS, fetal bovine serum; SD, standard deviation.

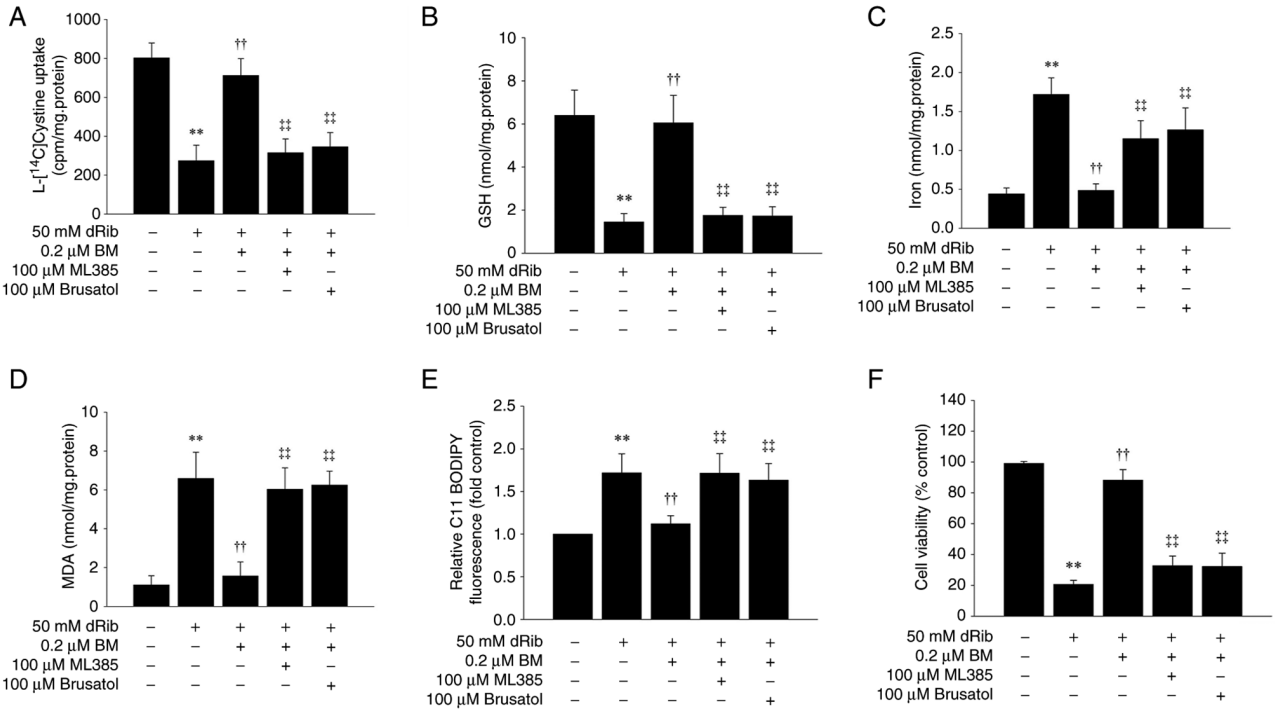

Figure 2. Effects of ML385 and brusatol on the protective effects of BM treatment on dRib-induced changes in (A) L-[^{14}C]cystine uptake, (B) intracellular GSH and (C) iron contents, (D) intracellular MDA, (E) lipid ROS levels and (F) cell viability. (A) NRK-52E cells were co-stimulated with 0.2 μM BM, 100 μM ML385, or 100 μM brusatol and 50 mM dRib for 4 h in the extracellular fluid buffer containing 1.7 μM L-[^{14}C]cystine (0.1 μCi/ml) at 37˚C. The radioactivity incorporated into the cells was determined by a liquid scintillation counter. (B-D and F) NRK-52E cells were co-stimulated with 0.2 μM BM, 100 μM ML385, or 100 μM brusatol and 50 mM dRib for 6 h in DMEM media containing 10% FBS. The intracellular GSH and iron levels, intracellular MDA levels, and cell viability were measured using a GSH assay kit, an iron assay kit, MDA assay kit, and LDH release assay kit, respectively. These experiments were performed thrice, in triplicate. (E) Intracellular lipid ROS level was quantified by flow cytometry using the lipophilic fluorescent dye C11-BODIPY. Cells were incubated with 4 μM C11-BODIPY during the final 30 min. Fold control of the mean fluorescence intensity of experimental groups. This experiment was performed four times. Data are presented as the mean ± SD. **P<0.01 vs. control; ††P<0.01 vs. 50 mM dRib-alone group; ‡‡P<0.01 vs. 50 mM dRib plus 0.2 μM BM group, as determined by one way analysis of variance and Tukey's post hoc test. BM, bardoxolone methyl; dRib, 2-deoxy-D-ribose; GSH, glutathione; MDA, malondialdehyde; ROS, reactive oxygen species.

The same results were observed in NRK-52E cells (Fig. 2A, B and F). In addition, the ability of BM to suppress intracellular iron, MDA, and C11-BODIPY fluorescence levels, which were elevated by dRib, was also counteracted by ML385 and brusatol (Figs. 2C-E and S2). These findings indicate that the ferroptosis-inhibitory effect of BM is dependent on Nrf2 activation.

BM increases the expression of SLC7A11 and Nrf2 target genes while reducing the expression of ferroptosis-related markers. Nrf2 protein expression was increased in a dose-dependent manner by dRib and was further enhanced by the addition of BM (Fig. 3A and B). Although Nrf2 mRNA expression was also increased dose-dependently by dRib, the addition of BM significantly suppressed the dRib-induced

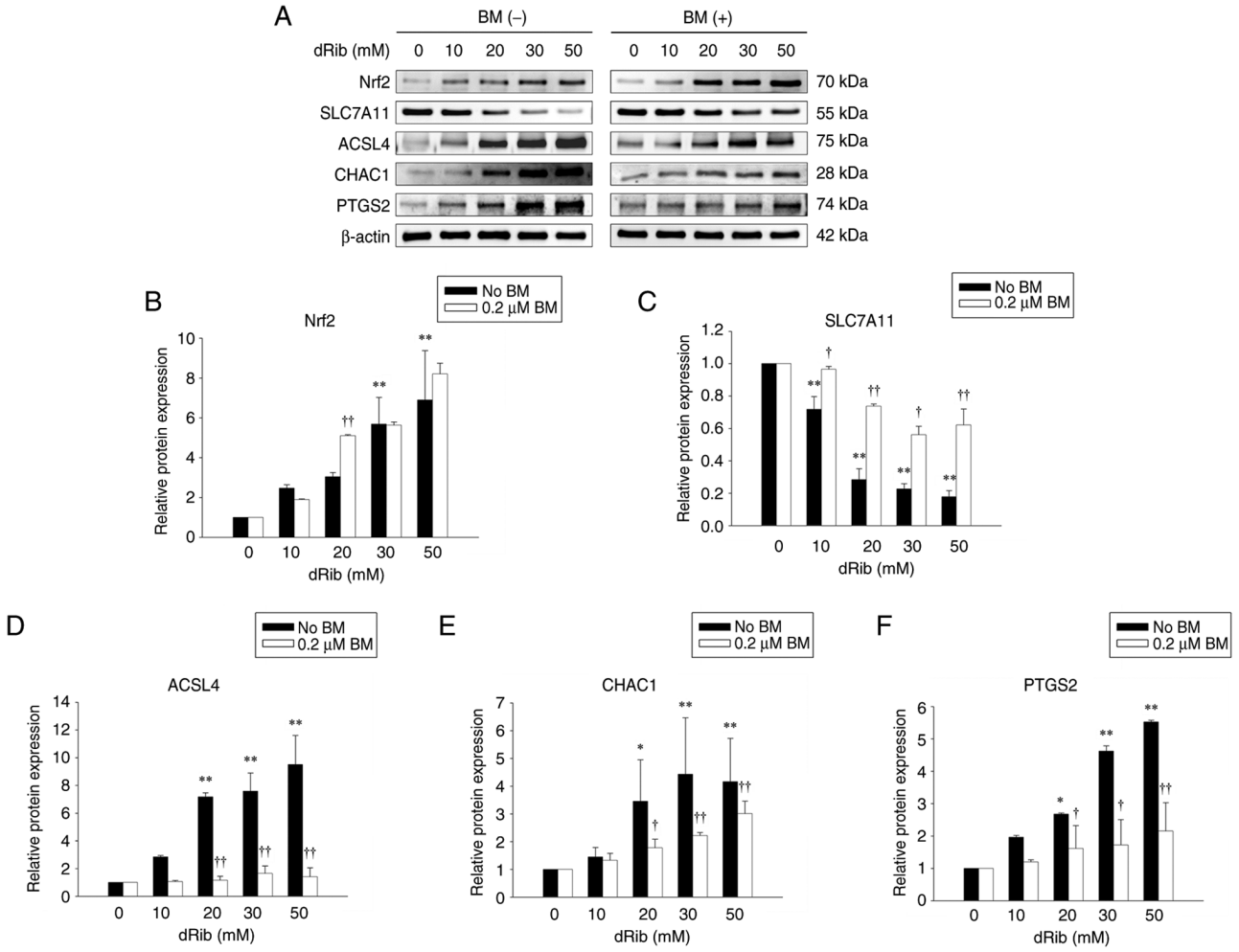

Figure 3. Effects of BM treatment on dRib-induced changes in Nrf2, SLC7A11, ACSL4, CHAC1 and PTGS2 protein expressions in NRK-52E cells after treatment with various concentrations of dRib. The cells were stimulated with 0, 10, 20, 30 or 50 mM dRib with or without 0.2 μM BM for 6 h in DMEM containing 10% FBS. The protein expression was analyzed by western blotting. β-Actin was used as loading control. (A) Representative blots of two independent experiments are shown. Densitometric quantification of (B) Nrf2, (C) SLC7A11, (D) ACSL4, (E) CHAC1 and (F) PTGS2 protein levels normalized to β-actin. Data are presented as the mean ± SD. *P<0.05 and **P<0.01 vs. 0 mM dRib group; †P<0.05 and ††P<0.01 vs. dRib alone, as determined by one-way analysis of variance and Tukey's post-hoc test or Welch's ANOVA followed by Dunnett's T3 post hoc test, depending on the result of Levene's test. SLC7A11, solute carrier family 7 member 11; ACSL4, acyl-CoA synthetase long chain family member 4; CHAC1, ChaC glutathione-specific gamma-glutamylcyclotransferase 1; PTGS2, prostaglandin-endoperoxide synthase 2; BM, bardoxolone methyl; dRib, 2-deoxy-D-ribose.

increase (Fig. 4A). Meanwhile, SLC7A11 protein, which is known to be degraded by dRib (7), showed a dose-dependent decrease upon dRib treatment, but this decrease was significantly prevented by BM (Fig. 3A and C).

We further examined the expression of Nrf2 target genes, including SLC7A11, HO-1, NQO1, the catalytic subunit of glutamate-cysteine ligase (GCLC), and the modifier subunit of glutamate-cysteine ligase (GCLM). These genes were upregulated by dRib and showed a further increase upon BM treatment. The BM-induced increase in these Nrf2 target genes was significantly attenuated by ML385 and brusatol (Figs. 4B and 5).

Next, we investigated the effect of BM on the expression of ferroptosis biomarkers. The mRNA and protein levels of ACSL4, ChaC glutathione-specific gamma-glutamylcyclotransferase 1 (CHAC1), and prostaglandin-endoperoxide synthase 2 (PTGS2) were all significantly increased by dRib in a dose-dependent manner. However, treatment with BM markedly reduced the expression of these ferroptosis-related markers (Figs. 3 and 4C-E). These regulatory effects on SLC7A11, ACSL4, CHAC1, and PTGS2 gene expression were also consistently observed in primary cultured rat RTECs (Fig. S3). These findings further support the notion that BM prevents ferroptosis by activating Nrf2 pathway.

BM disrupts Nrf2-Keap1 interaction and promotes the nuclear translocation of Nrf2. To elucidate the mechanism through which BM activates the Nrf2 pathway, we investigated the interaction between Nrf2 and Keap1 and their intracellular localization.

In the co-IP assay assessing their interaction, Keap1 was pulled down by Nrf2 in both the control and dRib-treated groups, indicating a physical association. However, when BM was added, the pull-down of Keap1 by Nrf2 was reduced (Fig. 6A and B). This indicates that although the physical interaction between Nrf2 and Keap1 remained intact under dRib treatment alone, the addition of BM weakened their association, implying that BM disrupts the Nrf2-Keap1 interaction.

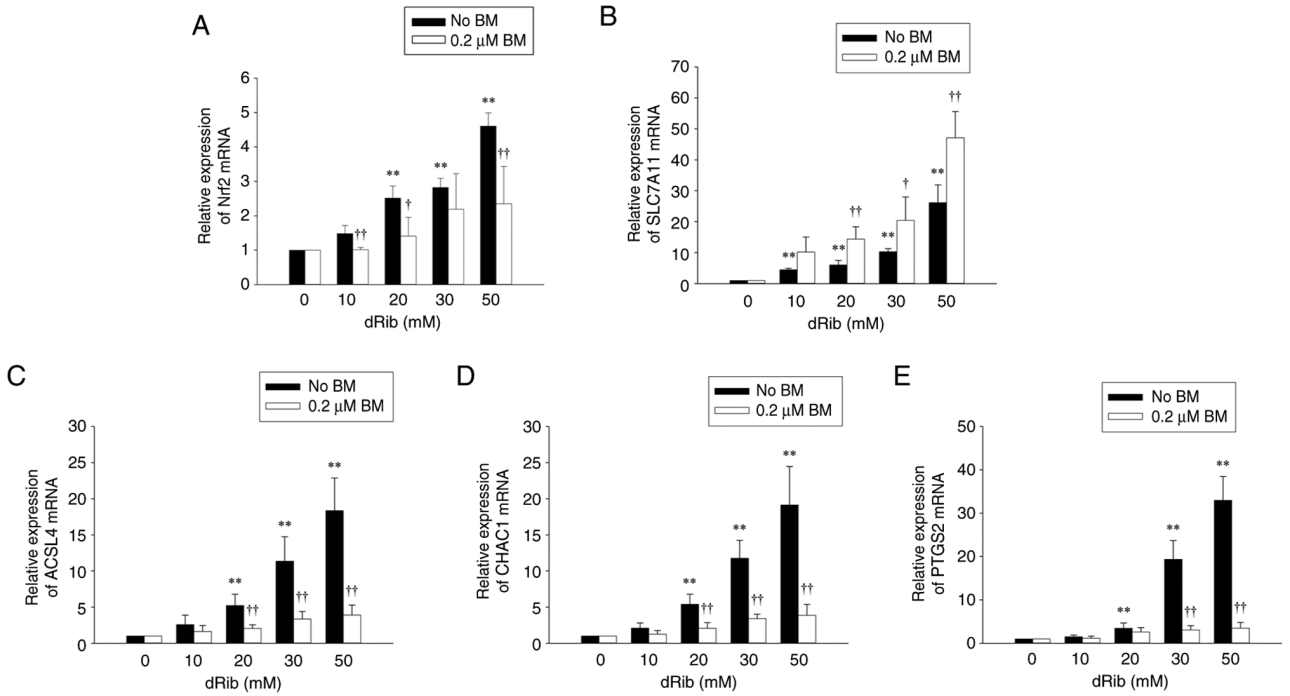

Figure 4. Effects of BM treatment on dRib-induced changes in (A) Nrf2, (B) SLC7A11, (C) ACSL4, (D) CHAC1 and (E) PTGS2mRNA expressions. NRK-52E cells were stimulated with 0, 10, 20, 30 or 50 mM dRib for 6 h in DMEM containing 10% FBS. The mRNA levels were analyzed by reverse transcription-quantitative polymerase chain reaction. Relative expression of target genes was calculated using the $2^{-\Delta\Delta Cq}$ method. This experiment was performed thrice, in triplicate. Data are presented as the mean ± SD. **P<0.01 vs. 0 mM dRib group; †P<0.05 and ††P<0.01 vs. dRib alone, as determined by one-way analysis of variance and Tukey's post-hoc test or Welch's ANOVA followed by Dunnett's T3 post hoc test, depending on the result of Levene's test. SLC7A11, solute carrier family 7 member 11; ACSL4, acyl-CoA synthetase long chain family member 4; CHAC1, ChaC glutathione-specific gamma-glutamylcyclotransferase 1; PTGS2, prostaglandin-endoperoxide synthase 2; BM, bardoxolone methyl; dRib, 2-deoxy-D-ribose.

To examine changes in the intracellular localization of Nrf2 and Keap1 upon dRib and BM treatment, we performed IF staining and observed the cells using confocal microscopy. In the control group, Nrf2 was evenly distributed between the cytoplasm and nucleus, whereas in the dRib-treated group, nuclear translocation of Nrf2 was increased. Notably, in the BM-treated group, nuclear translocation of Nrf2 was markedly enhanced, with minimal Nrf2 observed in the cytoplasm (Fig. 6C and D). However, Keap1 localization remained unchanged, as it was consistently retained in the cytoplasm regardless of dRib or BM treatment (Fig. S4). Results from co-IP and confocal microscopy indicate that BM disrupts the interaction between Nrf2-Keap1, thereby facilitating the nuclear translocation of Nrf2.

Discussion

In this study, we showed that BM inhibits ferroptosis in RTECs by activating the Nrf2 signaling pathway and upregulating SLC7A11 expression. These findings provide further insight into the renal protective mechanisms of BM in DKD and show a novel strategy to overcome the clinical limitations of current DKD treatments.

As ferroptosis is an iron-dependent form of oxidative cell death caused by lipid peroxidation, our finding that BM lowers intracellular iron levels and lipid peroxidation markers supports its role in preventing ferroptosis. This is further confirmed by BM's ability to reduce the expression of ferroptosis markers such as ACSL4, CHAC1, and PTGS2. ACSL4 promotes lipid peroxidation by catalyzing the esterification of polyunsaturated fatty acids (30). CHAC1 increases during ferroptosis triggered by system χc- inhibitors (31), and PTGS2 is a recognized marker of ferroptosis (32). BM inhibits ferroptosis mainly by increasing the expression of SLC7A11, which is essential for cystine transport through system χc^-. We found that BM raises both the mRNA and protein levels of SLC7A11, and also enhances cystine uptake and intracellular GSH levels. Notably, while dRib increased SLC7A11 mRNA expression, it decreased the protein levels. This matches our earlier work showing that dRib causes SLC7A11 protein degradation via the ubiquitin-proteasome pathway (7). This explains why SLC7A11 mRNA is upregulated as a compensatory response to reduced cystine uptake, but protein levels drop because of increased degradation. In contrast, BM activates Nrf2 and restores SLC7A11 protein levels, counteracting the degradation caused by dRib. Furthermore, the ferroptosis induced by dRib, which was prevented by BM, was primarily caused by impaired intracellular cystine transport (7). BM upregulates SLC7A11 by activating the Keap1-Nrf2 pathway. Keap1 normally inhibits Nrf2 activation (33). In our study, BM increased Nrf2 protein expression and promoted its intranuclear translocation by disrupting the interaction between Nrf2 and Keap1. Although BM does not directly enhance the transcription of Nrf2, it stabilizes the Nrf2 protein by interfering with its binding to Keap1, thereby inhibiting Keap1-mediated ubiquitination and proteasomal degradation of Nrf2 (20). As a result, Nrf2 accumulates in the cytoplasm and is subsequently translocated into the nucleus. Therefore, the observed

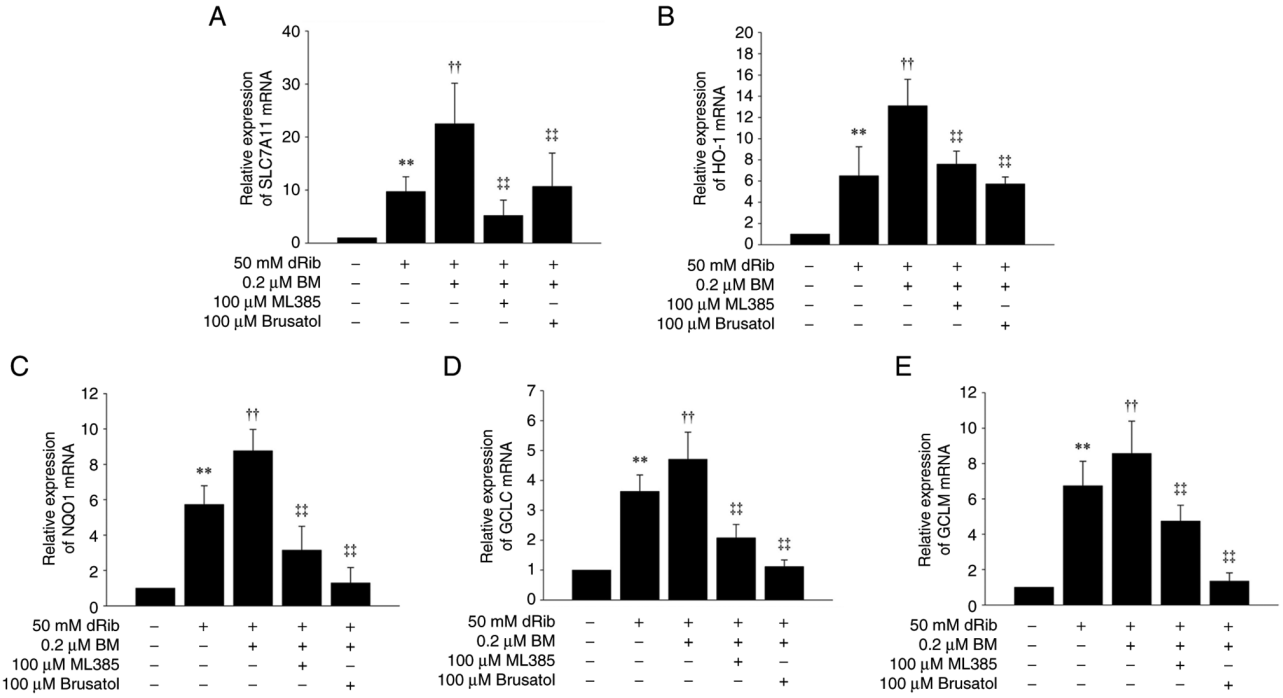

Figure 5. Effects of BM and ML385 or brusatol treatments on dRib-induced changes in SLC7A11 and Nrf2-antioxidant response element-dependent genes. NRK-52E cells were co-stimulated with 0.2 μM BM, 100 μM ML385, or 100 μM brusatol and 50 mM dRib for 6 h in DMEM containing 10% FBS. The mRNA levels of (A) SLC7A11, (B) HO-1, (C) NQO1, (D) GCLC and (E) GCLM were analyzed by reverse transcription-quantitative polymerase chain reaction. Relative expression of target genes was calculated using the $2^{-\Delta\Delta Cq}$ method. This experiment was performed thrice, in triplicate. Data are presented as the mean ± SD. **P<0.01 vs. control; ††P<0.01 vs. 50 mM dRib-alone group; ‡‡P<0.01 vs. 50 mM dRib plus 0.2 μM BM group, as determined by one way analysis of variance and Tukey's post hoc test. BM, bardoxolone methyl; dRib, 2-deoxy-D-ribose; SLC7A11, solute carrier family 7 member 11; GCLC, glutamate-cysteine ligase catalytic subunit; GCLM, glutamate-cysteine ligase modifier subunit; HO-1, heme oxygenase-1; NQO1, NADPH quinone oxidoreductase I.

increase in Nrf2 protein levels following BM treatment is primarily attributed to post-translational stabilization instead of increased gene expression. Consequently, the expression of Nrf2 target genes, including HO-1, NQO1, and GCL, was upregulated. Furthermore, the ferroptosis-inhibitory effects of BM were abolished by the Nrf2 inhibitors ML385 and brusatol, providing strong evidence that Nrf2 activation is essential for the protective effects of BM. Meanwhile, Nrf2 mRNA expression was increased by dRib, and this increase was prevented by the addition of BM. It is well known that Nrf2 mRNA expression increases in response to oxidative stress stimuli (34,35). Since BM promotes the stabilization of Nrf2 protein as described above, there is no need for increased transcription of Nrf2, and thus the addition of BM is thought to prevent the dRib-induced increase in Nrf2 mRNA expression.

BM has shown renoprotective effects in clinical trials involving patients with DKD; however, one trial failed to confirm these benefits. The BEACON trial, which aimed to verify the nephroprotective effects of BM in 2,185 patients with type 2 diabetes and reduced eGFR, was terminated early after only 9 months owing to an increased incidence of heart failure in the BM-treated group, thus preventing definitive confirmation of its kidney-protective effects (36). Subsequent studies conducted in Japanese patients with DKD, such as the TSUBAKI study (37) and the AYAME study (27), excluded patients with risk factors for heart failure. These studies revealed the nephroprotective effects of BM without significant adverse events. Therefore, heart failure remains a major obstacle in the development of BM as a therapeutic agent for DKD. Based on the results of our present study, a treatment strategy targeting SLC7A11 rather than BM, which activates Nrf2, may have the potential to prevent ferroptosis in RTECs while minimizing adverse effects. Therefore, the development of a novel compound that selectively upregulates SLC7A11 expression in RTECs could offer a safer and more effective therapeutic option for DKD. In addition to approaches targeting SLC7A11, other strategies may help reduce the cardiovascular risks associated with BM. First, tissue-specific drug delivery systems that selectively target the kidney can limit systemic exposure (38), thereby lowering the risk of off-target side effects such as heart failure. Second, combining BM with other renoprotective agents may allow for dose reduction, thereby improving its safety profile (39). Further research is required to develop structural analogs of BM (21) that retain Nrf2-activating capacity while reducing cardiotoxicity.

This study has some limitations. First, the concentration of dRib used in our study is considerably high. Erastin, a well-known system χ_c^- inhibitor, is typically used at micromolar concentrations, whereas we used dRib at concentrations of 10-50 mM. Unlike erastin, dRib is not a small molecule but rather a reducing sugar. Studies that have used reducing sugars to induce oxidative stress have consistently employed high concentrations, and some have even used concentrations higher than those used in our study (40,41). Second, it was conducted at the cellular level using NRK-52E cells and primary cultured RTECs. Therefore, it does not fully replicate the complex physiological environment of DKD, and further studies are required to verify whether similar results

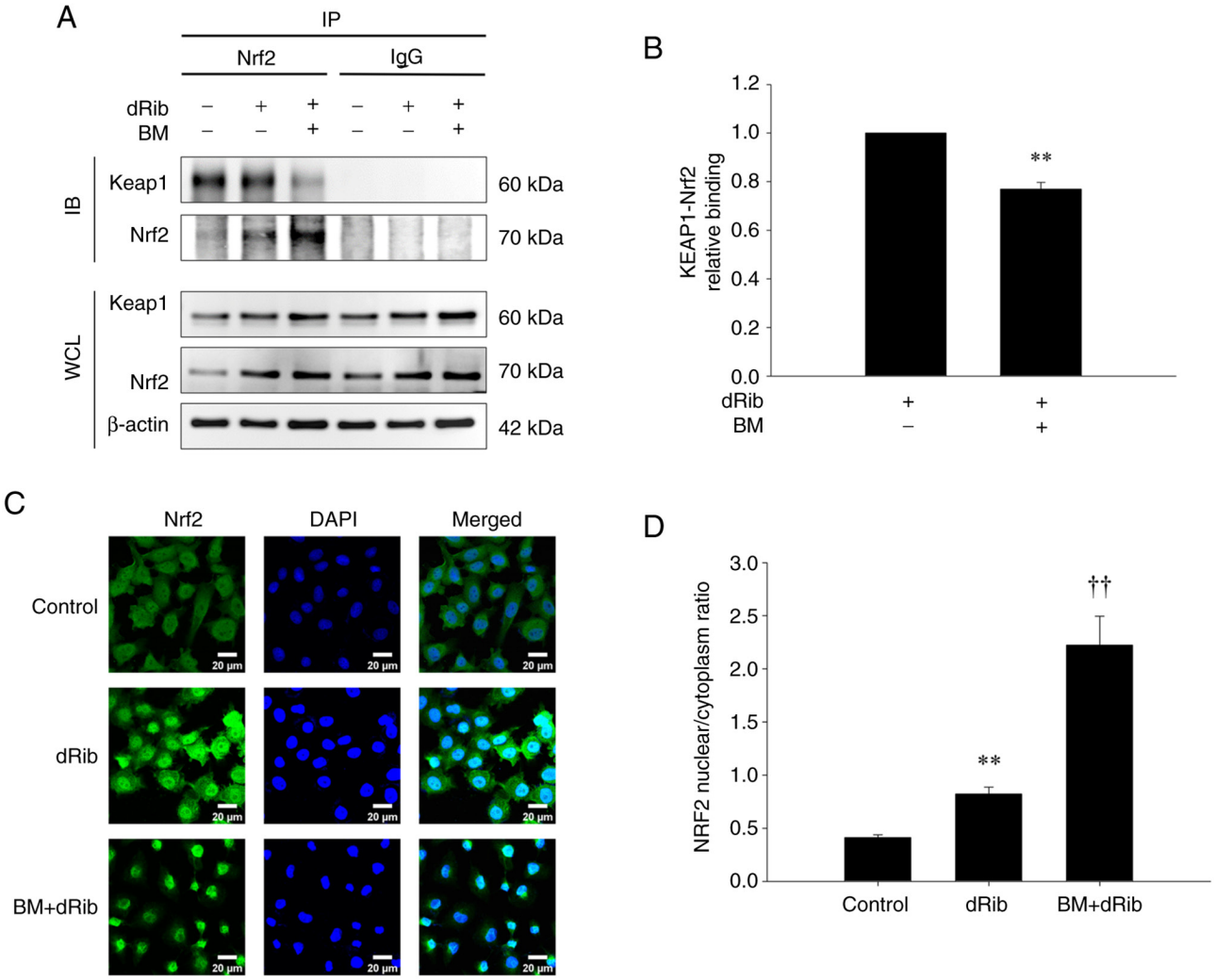

Figure 6. Investigation of Nrf2 and Keap1 interaction and intracellular localization using (A and B) co-IP and (C and D) immunofluorescence confocal microscopy. (A) NRK-52E cells were stimulated with 50 mM dRib with or without 0.2 μM BM for 6 h in DMEM media containing 10% FBS. The cell lysates were immunoprecipitated using an anti-Nrf2 antibody or control immunoglobulin (IgG), followed by IB with anti-Keap1 and anti-Nrf2 antibodies. The lower panels show IB of WCL. (B) Densitometric quantification of the immunoprecipitated Keap1 and Nrf2 protein bands from (A), normalized to IgG controls. Data represent the mean ± SD from three independent experiments. **P<0.01 vs. dRib alone, as determined by unpaired Student's t-test. (C) Cells were treated with dRib (50 mM) alone or in combination with BM (0.2 μM) for 6 h. Representative images from three independent experiments show Nrf2 (green), Keap1 (red), and DAPI (blue) staining, with merged images illustrating nuclear translocation of Nrf2 under different conditions. Scale bar=20 μm. (D) The nuclear/cytoplasmic ratio of Nrf2 expression was measured using the ImageJ program. Data are presented as the mean ± SD. **P<0.01 vs. control group; ††P<0.01 vs. dRib alone, as determined by one-way analysis of variance and Tukey's post-hoc test. BM, bardoxolone methyl; dRib, 2-deoxy-D-ribose; IB, immunoblotting; IP, immunoprecipitation; WCL, whole cell lysates.

are observed in animal models of DKD. Third, instead of using erastin, a widely used ferroptosis inducer, we induced ferroptosis in RTECs using dRib. However, both erastin and dRib induce ferroptosis through cysteine deprivation. Erastin inhibits system χc-, leading to a compensatory increase in SLC7A11 gene expression. Ferroptosis induced by erastin is known to be prevented by 2-mercaptoethanol, which bypasses system χc- to enhance cystine uptake (3). Similarly, dRib increases SLC7A11 gene expression in RTECs and enables dRib-induced ferroptosis to be prevented by 2-ME (7). Therefore, even if erastin had been used as a ferroptosis inducer, we believe the results would have been the same as those obtained in this study. Moreover, the reason we used dRib instead of erastin is that dRib is more suitable for *in vitro* studies using RTECs. Erastin does not dissolve well and is difficult to handle (42). In contrast, dRib dissolves readily in water, induces ferroptosis in RTECs in a dose-dependent manner, and its detailed mechanisms are well understood (7). For these reasons, we chose to use dRib in our study on ferroptosis in RTECs. Fourth, further research on intracellular signaling pathways that may contribute to the off-target effects of BM is required. Adverse effects of BM, such as heart failure, remain a major obstacle to its development as a therapeutic agent for DKD. Thus, elucidating these detailed mechanisms is as crucial as understanding the renoprotective mechanisms of BM, as it could contribute to the development of an optimal DKD treatment.

This study showed that BM inhibits ferroptosis in renal tubular epithelial cells by activating the Keap1-Nrf2 pathway and increasing the expression of SLC7A11. BM reversed the dRib-induced decrease in cystine uptake, GSH depletion, intracellular iron accumulation, and lipid peroxidation, and

these effects were noted to be dependent on Nrf2 activation. Although BM appears to be a promising therapeutic strategy for DKD, adverse effects such as heart failure remain a significant concern. Future research should focus on developing safer therapeutic agents that selectively enhance SLC7A11 activity to inhibit ferroptosis.

Acknowledgements

Not applicable.

Funding

This work was supported by a research grant from Jeju National University Hospital in 2023.

Availability of data and materials

The data generated in the present study may be requested from the corresponding author.

Authors' contributions

GK, SAL and MK conceived and designed the research. GK, JYB and SY performed experiments. GK and SY analyzed data. GK, JYB and SY interpreted results of experiments. GK and SAL acquired funding. GK, JYB and SY confirm the authenticity of all the raw data. GK, JYB and SY prepared figures. GK, SY and MK drafted the manuscript, and GK edited and revised the manuscript. All authors read and approved the final manuscript.

Ethics approval and consent to participate

The present study was approved by the Institutional Animal Care and Use Committee of Jeju National University (approval no. 2022-0014).

Patient consent for publication

Not applicable.

Competing interests

The authors declare that they have no competing interests.

References

1. Li J, Cao F, Yin HL, Huang ZJ, Lin ZT, Mao N, Sun B and Wang G: Ferroptosis: Past, present and future. Cell Death Dis 11: 88, 2020.
2. Zhu J, Xiong Y, Zhang Y, Wen J, Cai N, Cheng K, Liang H and Zhang W: The molecular mechanisms of regulating oxidative stress-induced ferroptosis and therapeutic strategy in tumors. Oxid Med Cell Longev 2020: 8810785, 2020.
3. Dixon SJ, Lemberg KM, Lamprecht MR, Skouta R, Zaitsev EM, Gleason CE, Patel DN, Bauer AJ, Cantley AM, Yang WS, *et al*: Ferroptosis: An iron-dependent form of nonapoptotic cell death. Cell 149: 1060-1072, 2012.
4. Yan HF, Zou T, Tuo QZ, Xu S, Li H, Belaidi AA and Lei P: Ferroptosis: Mechanisms and links with diseases. Signal Transduct Target Ther 6: 49, 2021.
5. Zilka O, Shah R, Li B, Friedmann Angeli JP, Griesser M, Conrad M and Pratt DA: On the mechanism of cytoprotection by ferrostatin-1 and liproxstatin-1 and the role of lipid peroxidation in ferroptotic cell death. ACS Cent Sci 3: 232-243, 2017.
6. Dringen R and Hirrlinger J: Glutathione pathways in the brain. Biol Chem 384: 505-516, 2003.
7. Kim M, Bae JY, Yoo S, Kim HW, Lee SA, Kim ET and Koh G: 2-Deoxy-D-ribose induces ferroptosis in renal tubular epithelial cells via ubiquitin-proteasome system-mediated xCT protein degradation. Free Radic Biol Med 208: 384-393, 2023.
8. Stockwell BR, Friedmann Angeli JP, Bayir H, Bush AI, Conrad M, Dixon SJ, Fulda S, Gascón S, Hatzios SK, Kagan VE, *et al*: Ferroptosis: A regulated cell death nexus linking metabolism, redox biology, and disease. Cell 171: 273-285, 2017.
9. Yao MY, Liu T, Zhang L, Wang MJ, Yang Y and Gao J: Role of ferroptosis in neurological diseases. Neurosci Lett 747: 135614, 2021.
10. ElSayed NA, Aleppo G, Aroda VR, Bannuru RR, Brown FM, Bruemmer D, Collins BS, Hilliard ME, Isaacs D, Johnson EL, *et al*: 11. chronic kidney disease and risk management: standards of care in diabetes-2023. Diabetes Care 46 (Suppl 1): S191-S202, 2023.
11. Barnett AH, Bain SC, Bouter P, Karlberg B, Madsbad S, Jervell J and Mustonen J; Diabetics Exposed to Telmisartan and Enalapril Study Group: Angiotensin-receptor blockade versus converting-enzyme inhibition in type 2 diabetes and nephropathy. N Engl J Med 351: 1952-1961, 2004.
12. Solomon J, Festa MC, Chatzizisis YS, Samanta R, Suri RS and Mavrakanas TA: Sodium-glucose co-transporter 2 inhibitors in patients with chronic kidney disease. Pharmacol Ther 242: 108330, 2023.
13. Yang XD and Yang YY: Ferroptosis as a novel therapeutic target for diabetes and its complications. Front Endocrinol (Lausanne) 13: 853822, 2022.
14. Zhang X and Li X: Abnormal iron and lipid metabolism mediated ferroptosis in kidney diseases and its therapeutic potential. Metabolites 12: 58, 2022.
15. Kim S, Kang SW, Joo J, Han SH, Shin H, Nam BY, Park J, Yoo TH, Kim G, Lee P and Park JT: Characterization of ferroptosis in kidney tubular cell death under diabetic conditions. Cell Death Dis 12: 160, 2021.
16. Mengstie MA, Seid MA, Gebeyehu NA, Adella GA, Kassie GA, Bayih WA, Gesese MM, Anley DT, Feleke SF, Zemene MA, *et al*: Ferroptosis in diabetic nephropathy: Mechanisms and therapeutic implications. Metabol Open 18: 100243, 2023.
17. Wang Y, Bi R, Quan F, Cao Q, Lin Y, Yue C, Cui X, Yang H, Gao X and Zhang D: Ferroptosis involves in renal tubular cell death in diabetic nephropathy. Eur J Pharmacol 888: 173574, 2020.
18. Wang WJ, Jiang X, Gao CC and Chen ZW: Salusin-β participates in high glucose-induced HK-2 cell ferroptosis in a Nrf-2-dependent manner. Mol Med Rep 24: 674, 2021.
19. Li S, Zheng L, Zhang J, Liu X and Wu Z: Inhibition of ferroptosis by up-regulating Nrf2 delayed the progression of diabetic nephropathy. Free Radic Biol Med 162: 435-449, 2021.
20. Rojas-Rivera J, Ortiz A and Egido J: Antioxidants in kidney diseases: The impact of bardoxolone methyl. Int J Nephrol 2012: 321714, 2012.
21. Wang YY, Yang YX, Zhe H, He ZX and Zhou SF: Bardoxolone methyl (CDDO-Me) as a therapeutic agent: An update on its pharmacokinetic and pharmacodynamic properties. Drug Des Devel Ther 8: 2075-2088, 2014.
22. Suzuki T and Yamamoto M: Molecular basis of the Keap1-Nrf2 system. Free Radic Biol Med 88 (Pt B): 93-100, 2015.
23. Yu H, Guo P, Xie X, Wang Y and Chen G: Ferroptosis, a new form of cell death, and its relationships with tumourous diseases. J Cell Mol Med 21: 648-657, 2017.
24. Pergola PE, Krauth M, Huff JW, Ferguson DA, Ruiz S, Meyer CJ and Warnock DG: Effect of bardoxolone methyl on kidney function in patients with T2D and Stage 3b-4 CKD. Am J Nephrol 33: 469-476, 2011.
25. Nangaku M, Takama H, Ichikawa T, Mukai K, Kojima M, Suzuki Y, Watada H, Wada T, Ueki K, Narita I, *et al*: Randomized, double-blind, placebo-controlled phase 3 study of bardoxolone methyl in patients with diabetic kidney disease: Design and baseline characteristics of the AYAME study. Nephrol Dial Transplant 38: 1204-1216, 2023.
26. Pergola PE, Raskin P, Toto RD, Meyer CJ, Huff JW, Grossman EB, Krauth M, Ruiz S, Audhya P, Christ-Schmidt H, *et al*: Bardoxolone methyl and kidney function in CKD with type 2 diabetes. N Engl J Med 365: 327-336, 2011.
27. Tadao A, Kengo Y, Tomohiro I, Kazuya M and Masaomi N: AYAME Study: Randomized, Double-Blind, Placebo-Controlled Phase 3 Study of Bardoxolone Methyl in Diabetic Kidney Disease (DKD) Patients FR-OR110. JASN 34: pB1, 2023.

28. Kanda H and Yamawaki K: Bardoxolone methyl: Drug development for diabetic kidney disease. Clin Exp Nephrol 24: 857-864, 2020.
29. Bustin SA, Benes V, Garson JA, Hellemans J, Huggett J, Kubista M, Mueller R, Nolan T, Pfaffl MW, Shipley GL, *et al*: The MIQE guidelines: Minimum information for publication of quantitative real-time PCR experiments. Clin Chem 55: 611-622, 2009.
30. Ye L, Jin F, Kumar SK and Dai Y: The mechanisms and therapeutic targets of ferroptosis in cancer. Expert Opin Ther Targets 25: 965-986, 2021.
31. Dixon SJ, Patel DN, Welsch M, Skouta R, Lee ED, Hayano M, Thomas AG, Gleason CE, Tatonetti NP, Slusher BS and Stockwell BR: Pharmacological inhibition of cystine-glutamate exchange induces endoplasmic reticulum stress and ferroptosis. Elife 3: e02523, 2014.
32. Chen X, Comish PB, Tang D and Kang R: Characteristics and biomarkers of ferroptosis. Front Cell Dev Biol 9: 637162, 2021.
33. Hayes JD, Dayalan Naidu S and Dinkova-Kostova AT: Regulating Nrf2 activity: Ubiquitin ligases and signaling molecules in redox homeostasis. Trends Biochem Sci 50: 179-205, 2025.
34. Taqi MO, Saeed-Zidane M, Gebremedhn S, Salilew-Wondim D, Tholen E, Neuhoff C, Hoelker M, Schellander K and Tesfaye D: NRF2-mediated signaling is a master regulator of transcription factors in bovine granulosa cells under oxidative stress condition. Cell Tissue Res 385: 769-783, 2021.
35. Zeng XP, Li XJ, Zhang QY, Liu QW, Li L, Xiong Y, He CX, Wang YF and Ye QF: Tert-butylhydroquinone protects liver against ischemia/reperfusion injury in rats through Nrf2-activating anti-oxidative activity. Transplant Proc 49: 366-372, 2017.
36. de Zeeuw D, Akizawa T, Audhya P, Bakris GL, Chin M, Christ-Schmidt H, Goldsberry A, Houser M, Krauth M, Lambers Heerspink HJ, *et al*: Bardoxolone methyl in type 2 diabetes and stage 4 chronic kidney disease. N Engl J Med 369: 2492-2503, 2013.
37. Nangaku M, Kanda H, Takama H, Ichikawa T, Hase H and Akizawa T: Randomized clinical trial on the effect of bardoxolone methyl on GFR in diabetic kidney disease patients (TSUBAKI Study). Kidney Int Rep 5: 879-890, 2020.
38. Lu Y, Aimetti AA, Langer R and Gu Z: Bioresponsive materials. Nat Rev Mater 2: 16075, 2017.
39. Alicic RZ, Neumiller JJ and Tuttle KR: Combination therapy: An upcoming paradigm to improve kidney and cardiovascular outcomes in chronic kidney disease. Nephrol Dial Transplant 40 (Supplement 1): i3-i17, 2025.
40. Kaneto H, Fujii J, Myint T, Miyazawa N, Islam KN, Kawasaki Y, Suzuki K, Nakamura M, Tatsumi H, Yamasaki Y and Taniguchi N: Reducing sugars trigger oxidative modification and apoptosis in pancreatic beta-cells by provoking oxidative stress through the glycation reaction. Biochem J 320 (Pt 3): 855-863, 1996.
41. Tanaka Y, Tran PO, Harmon J and Robertson RP: A role for glutathione peroxidase in protecting pancreatic beta cells against oxidative stress in a model of glucose toxicity. Proc Natl Acad Sci USA 99: 12363-12368, 2002.
42. Wang L, Chen X and Yan C: Ferroptosis: An emerging therapeutic opportunity for cancer. Genes Dis 9: 334-346, 2020.